ANNALI DI GEOFISICA, VOL. 41, N. 2, June 1998

Interpretation of VLF-EM anomalies of 3D structures by using linear filtering techniques

Mohamed Djeddi([1])([2]), **Haydar A. Baker**([2]) **and Alain Tabbagh**([1])
([1]) *Centre de Recherche Géophysique, Garchy, France*
([2]) *Département de Géophysique, IST, USTHB, Alger, Algeria*

Abstract
For almost four decades now, the VLF-EM method has been used to locate different conducting structures. The interpretation is usually carried out on a profile anomaly where a possible estimation of the depth and the dip can be obtained. The maps are only used, after applying the Fraser filter, to best position the anomaly and no further quantitative interpretation is given. In this paper a linear filtering technique is developed based on the *X*- and *Y*-derivatives of the VLF-EM anomaly. This technique helps in determining the exact dimensions of the causative structures as well as their depths regardless of their conductivities. This work also shows that the known Fraser filter that is usually applied on a profile data can be adapted, for the first time, in studying quantitatively 3D structures if it is applied to raw data in the *X*- and *Y*-directions. It can now be used to estimate the dimensions of the targets.

Key words *VLF-EM – fraser filter – linear filtering – 3D interpretation*

1. Introduction

In the 1960s the VLF-EM technique was especially developed with the use of the transmitted signals of the already established powerful radio communication stations (in the 10-30 kHz band). The transmitters of these stations generate primary fields with horizontal magnetic components (H_y), and vertical electric component (E_z). Both components are perpendicular to the direction of propagation (X). At great distance, their wave front is considered uniform and plane. It is known that the induction caused by the primary magnetic field in a homogenous earth modifies the H_y component and creates a horizontal electric component E_x, and when a subsurface conductor is encountered, a secondary magnetic field (H_s) will be generated (fig. 1).

The VLF-EM technique has been widely used in mining exploration (Paterson and Ronka, 1971) as well as in underground water prospecting. In this technique, the real and imaginary parts of the ratio H_z/H_y are measured, where H_z is the vertical component of the secondary magnetic field that appears with non horizontal discontinuity present in the prospected area. H_y is considered here as the horizontal component of the total magnetic field.

During the last 30 years several methods, both analogue and numerical, have been developed by many researchers to interpret the VLF-EM data and attempts have been made to determine the parameters of heterogeneities.

Mailing address: Dr. Haydar A. Baker, 18 Rue du Hoggar, Hydra 16035, Alger, Algeria; e-mail: usthbist2@ist.cerist.dz

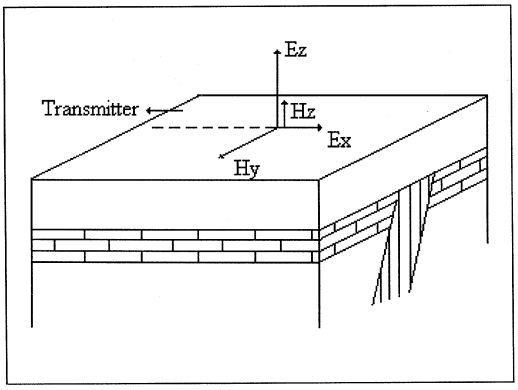

Fig. 1. Field components for a VLF transmitter at a great distance.

Coney (1977) and Baker and Myers (1979) based their studies principally on analogue models. Fraser (1969) proposed the horizontal gradient filter. Karous and Hjelt (1983) presented the current density cross-section. Ogilvy and Lee (1991) evaluated the performance of Karous filter. Recently Chouteau *et al.* (1996) used Maxwell's equations to obtain an autoregressive filter to convert the VLF-EM measurements into apparent resistivity data. Tabbagh *et al.* (1991) working on VLF resistivity showed that, when the VLF transmitters are used, the polarisation of the primary field introduces an apparent anisotropy that appears as an extension lateral of the anomalies in a direction perpendicular to the propagation direction. To minimise the effect of the apparent anisotropy, they proposed the verticalization of the electric field technique in which the variation of the secondary vertical electric field is calculated directly from the variations of the secondary horizontal electric field. Later on, Guerin *et al.* (1994), in their study of the field polarisation effect in MT-VLF, proposed a new technique that transforms the raw data of apparent MT-VLF resistivity into a map, which reflects the lateral variations of the ground resistivity and corrects spurious orientation effect due to the polarisation of the primary field.

It is an accepted fact that most of the ground VLF-EM anomalies are caused by the galvanic effect (McNeil, 1985) where the influence of frequency may be neglected (Guerin *et al.*, 1994). In this case, we can assume that it is possible to apply the potential field transformations used in magnetic and gravity surveys to VLF-EM data. Therefore, in our approach, we use a filter which is mainly based on the differential operator properties, in order to enhance the hidden features of a given signal. For this purpose the horizontal derivatives in X- and Y-directions are used. It can easily be shown that the derivation of the data in the space domain is equivalent to a product of the Fourier transform of data, multiplied by $-2i\pi u$ and $-2i\pi v$ respectively, in the spectral domain. In this paper we consider the magnetic field H_y to be directed along the Y-axis and that the electric field follows the X-axis. Furthermore, and for the theoretical calculation and interpretation, the real component data computed by a 3D modelling were tested only, because in practice the component in quadrature (Q) or the imaginary part of H_s/H_y is less reliable, as it is affected by the overburden and it is usually smaller than the in-phase component (P) or the real part of H_s/H_y.

Finally, in proposing this method, one can determine the exact limits of a buried body without considering its conductivity.

2. Model characteristics

To obtain 3D synthetic data we used the model shown in fig. 2a, a model generally found in shallow depth electromagnetic prospecting, which is a conductive body embedded in a homogenous medium that overlies a resistive substratum. The real part component of the normalised vertical magnetic field is computed at 20 kHz using the integral equation modelling program (Tabbagh, 1985). In this program the electromagnetic integral equations are approximated by dividing the whole body into n-number of cubic or parallelepipedic cells (fig. 2b). In each cell, the field is assumed constant and equal to its value in the centre of the cell. The value of the electromagnetic field at the surface is computed by adding the effect of all the cells. The results are shown in fig. 3, for two bodies with different dimensions.

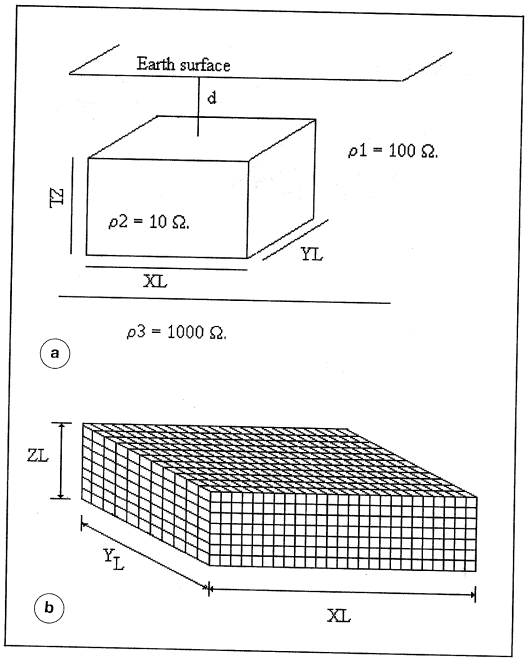

Fig. 2a,b. a) The 3D model used in the integral equation modelling. The conductive body is embedded in homogenous medium surmounting a resistive substratum; b) the body with a cubic discretization.

3. Aspect and application of filter

Let f be a 2D harmonic function defined in a domain $\wp$ which is in this case a horizontal surface (xoy). The measurements are performed at a constant level z outside the sources. If we define $\tilde{f}$ as the Fourier transform of f, then it can easily be shown that the derivatives $\frac{\partial f}{\partial X}$ (or $f'x$) and $\frac{\partial f}{\partial Y}$ (or $f'y$) are related to the initial function by the following relationships:

$$TF\left(\frac{\partial f}{\partial X}\right) = (-2\,i\,\pi u)\tilde{f}$$
$$TF\left(\frac{\partial f}{\partial Y}\right) = (-2\,i\,\pi v)\tilde{f} \qquad (3.1)$$

where u and v are spatial frequencies in the spectral domain.

Let us write

$$G(u) = -2\,i\,\pi u$$
$$G(v) = -2\,i\,\pi v \qquad (3.2)$$

These operators can be considered in the spectral domain as a linear filter.

$G(u)$ and $G(v)$ can readily be rewritten using Euler notation as:

$$G(u) = 2\,\pi|u|\exp(-i\,\pi/2)$$
$$G(v) = 2\,\pi|v|\exp(-i\,\pi/2) \qquad (3.3)$$

Equation (3.3) shows that the transformed functions $f'x$ and $f'y$ are phase shifted by $\pi/2$.

Therefore, in the space domain each maximum is transformed into zero value and each inflexion point into peak or trough. This is very well demonstrated by the derivation of VLF-EM data. In considering the derivatives in the X and Y-directions, two possible cases appear. The first, when the body is striking parallel to E_x, while the second is for a body having a strike perpendicular to E_x.

3.1. *X-Derivative* (first case)

It is clearly noted that when the X-derivative applied to VLF-EM maps of fig. 3 (each has a peak and a trough), it transforms these maps into X-derivative ones with four extremities (two peaks and two troughs) (fig. 4). In this case each part of the original VLF-EM anomaly (negative or positive) is transformed into peak and trough separated by a zero line. This is mainly due to the high gradient normally observed near the edges of the body.

From the first observation it is noted that, the four extremities indicate the approximate limits of the body in the XY plane and that the dispositions of these extremities show the strike direction of the target.

The distance between the peak and the trough along the X direction gives the limits of

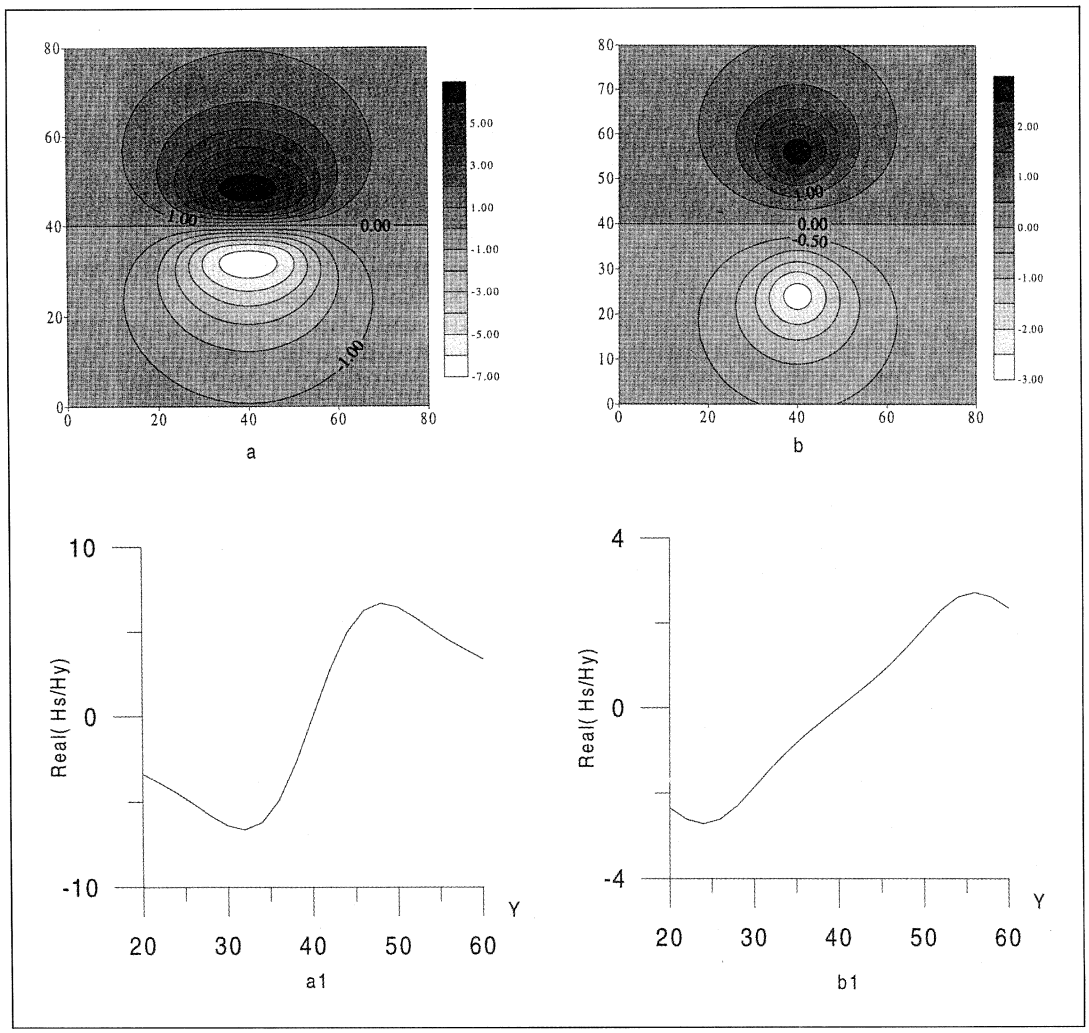

Fig. 3. VLF-EM Real component (H_s/H_y) maps (*a* and *b*) and profiles (a_1 and b_1). *a* for a conducting body with $XL = 30$, $YL = 10$, $ZL = 6$; *b* for a conducting body with $XL = 10$, $YL = 30$, $ZL = 6$.

the body which directly indicates its dimension along the *X*-axis (fig. 4). Furthermore, the zero contour lines represent the symmetry axes of the body in the *XY* plane. Moreover, the distance between the two extremities along the *Y*-direction is in fact the same as that of the peak-to-peak anomaly observed on a typical VLF-EM anomaly map, which is commonly used to estimate the depth to top of targets.

3.2. *Y-Derivative* (first case)

In this derivation along the *Y*-direction (fig. 5), the two extremities observed on the VLF-EM map have disappeared and the transformed maps show three extremities, which are also related to the high gradients near the edges of the body along the *Y* direction. Of the three extremities (one maximum and two min-

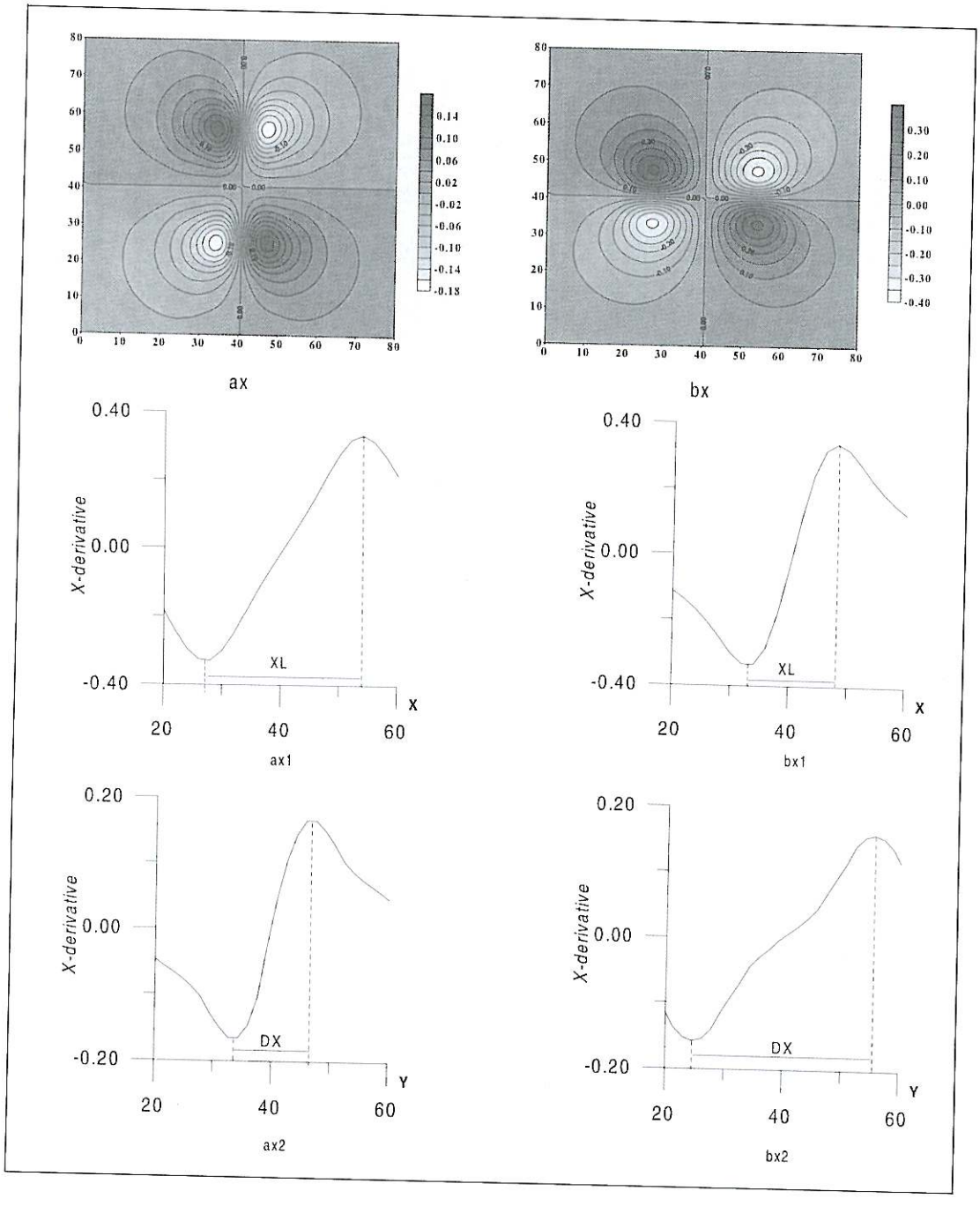

Fig. 4. a_x and b_x are the X-derivative maps of the Real (H_x/H_y) of corresponding bodies in fig. 3. a_{x1} = Profile at $Y = 35$; b_{x1} = profile at $Y = 25$; a_{x2} = profile at $X = 25$; b_{x2} = profile at $X = 35$.

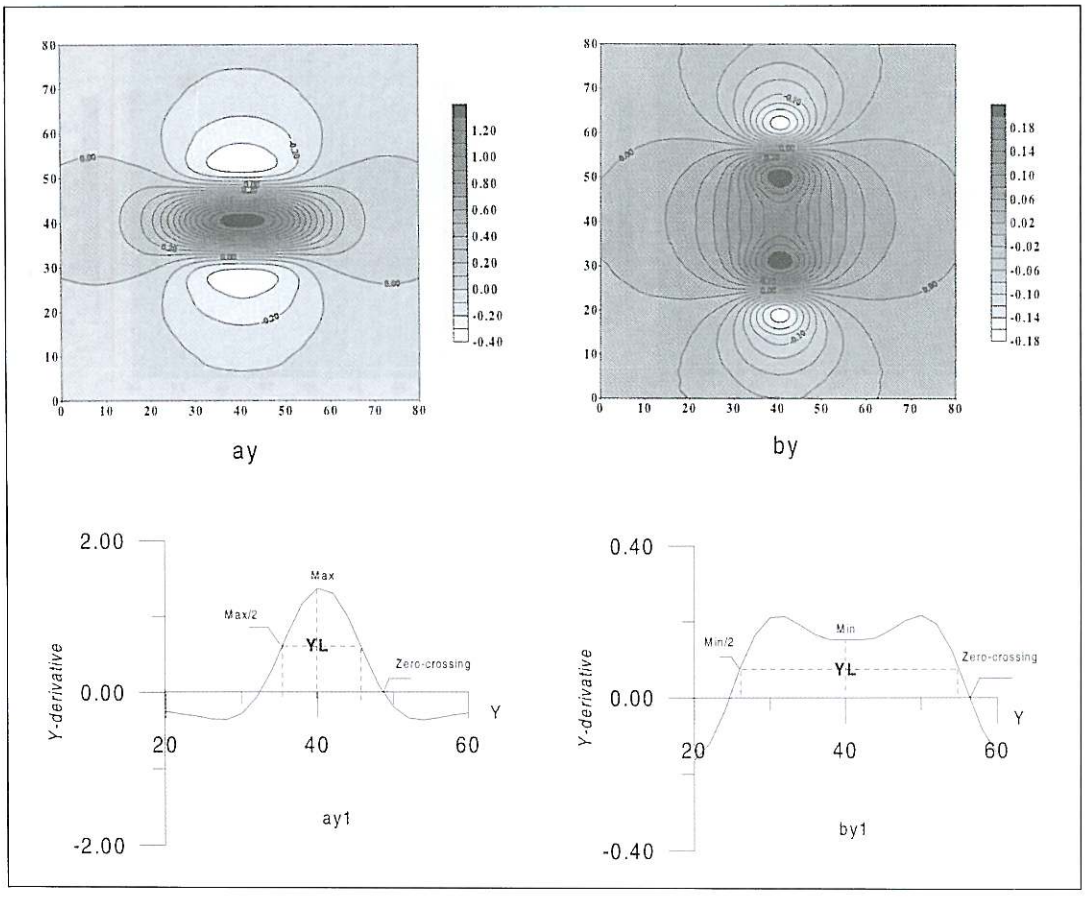

Fig. 5. a_y and b_y are the Y-derivative maps of the Real (H_x/H_y) of corresponding bodies in fig. 3. A_{y1} = profile at $X = 40$; b_{y1} = profile at $X = 40$.

ima in the case of a conducting body), the middle one is always centred above the body. This extremity also gives the limits and the extension of the body following the Y direction.

In order to obtain the exact extension, a profile has to be drawn passing through the three extremities (fig. 5.a_{y1} and 5.b_{y1}). In a similar manner to the one used in the gravity method, the half-value of the central intensity would give the exact extension of the body in the Y-direction. Furthermore, the distance between the zero crossings observed on these profiles is the same as that of the peak-to-peak one of the VLF-EM map.

3.3. *X- and Y-derivatives* (second case)

In case the body strike is perpendicular to E_x. The same phenomena of extremities are also observed and their dispositions in the X- and Y-directions clearly reflect all the dimensions of the causative structures. However, the central observed value in the Y-derivative will not be a maximum, but rather a relative minimum with respect to the two adjacent extremities. This can be explained as being due to somewhat constant field values over the central part of the elongated structure.

4. Application of fraser filter to 3D model studies

It is known that the Fraser filter which is used in the VLF-EM interpretation changes the crossover point of a profile into maximum. Then all the transformed profiles are laid on a map and only positive values are considered. The Fraser filter has always been used to give a better location of conductive targets and also some simple qualitative interpretation can be carried out. But it has never been used in the study of 3D bodies to obtain quantitative results, which include the depth, width and length of the causative structures.

The Fraser filter, by definition, could be considered as a first derivative. Therefore, in testing its possible applicability in studying 3D

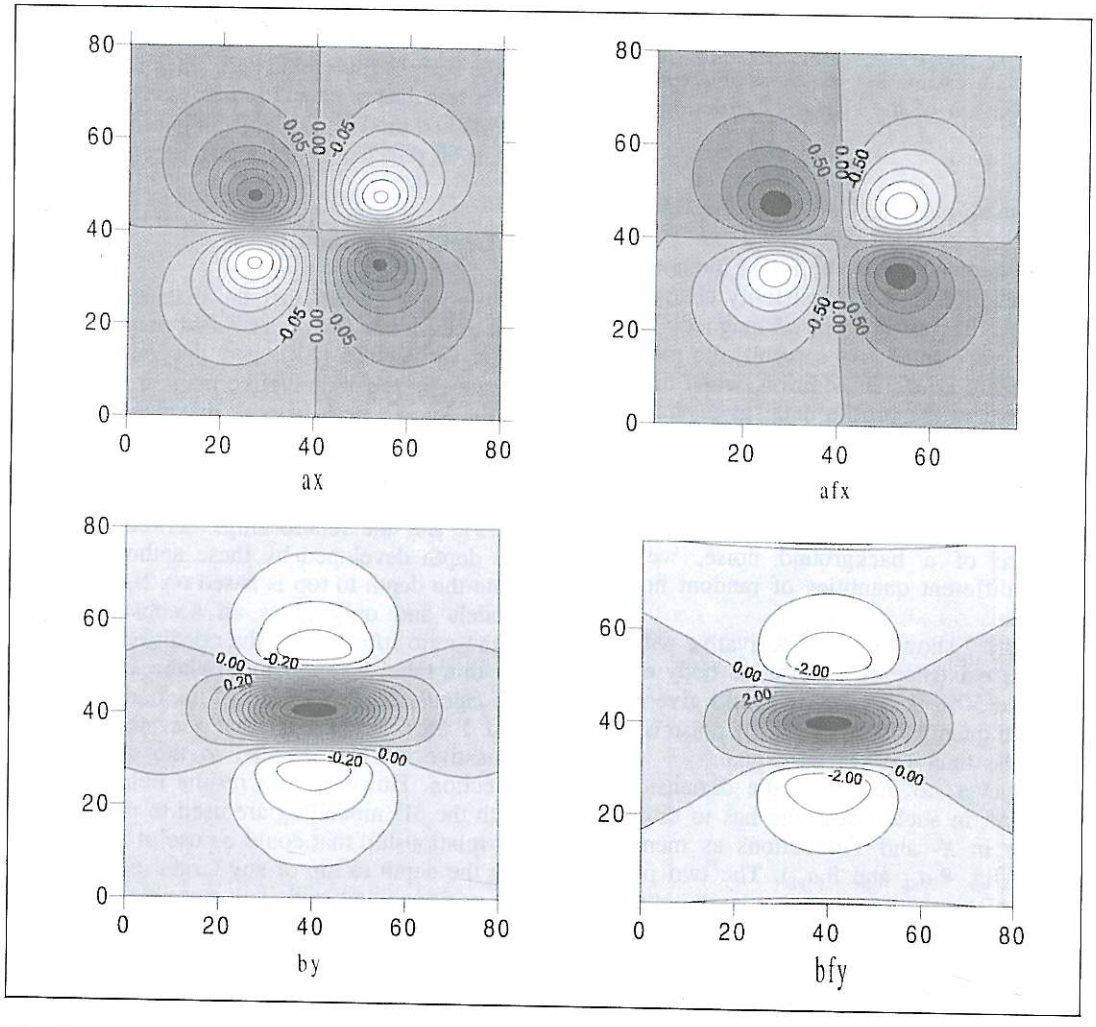

Fig. 6. Comparison between the X- and Y-derivative maps and the suggested application of the Fraser filter in the X and Y directions. a_x and b_y are the X and Y-derivatives; a_{fx} and b_{fy} are the Fraser filters.

structures, we applied the Fraser filter in the X and Y directions to non filtered VLF-EM data map, and compared the results with those obtained by applying the above proposed filter in the same directions. The results obtained are strikingly similar (fig. 6), where the application of the Fraser filter in the X-direction gives four extremities as those obtained by the X-derivative, and its application in the Y-direction gives a maximum above the target (for a conducting body).

Consequently, at this point, we can say that even the Fraser filter can be used in a similar way to the one presented in this paper, in order to have an estimation of the depth, width and the extension of the causative structures.

5. Noise/signal effect on filter application

It is known that the VLF-EM method is not very sensitive to small resistivity changes and that the observed normalised magnetic field is usually very small. As a result, the measured profiles are noisy. In addition, when the filter is applied to the profile data, more noise will theoretically be added because the filter itself is also susceptible to high frequency noise, as it is a differential operator. Therefore, and in order to test the applicability of our filter in the presence of a background noise, we have added different quantities of random noise to our data.

Figure 7 shows that the derivative will indicate the existence of a causative body even if we have 50% noise, and it would give an acceptable quantitative result if the noise is equal to or less than 15% of the signal.

However, to determine the dimensions of the target in such cases, one has to draw two profiles in X- and Y-directions as mentioned above (fig. 8.a_{x1} and 8.a_{y1}). The two profiles show noisy curves and cannot be directly used to obtain the extensions of the body and thus the data of the profile have to be smoothed and this can easily be done by choosing a good interpolation function. The interpolated profiles (fig. 8.a_{x2} and 8.a_{y2}) can then be used to determine the dimensions of the body.

6. Depth effect

It is known that the VLF-EM response of a body is inversely proportional to its depth to top. Therefore, several models have been tested at different depths and the dimensions of each model have been computed in each case, table I shows some of the results obtained.

We noted that in all cases a good determination of the horizontal dimensions of the causative body depends on the relation between the depth to top of the body and its smallest extension in the XY-plane. This means that the determination of the smallest extension of the body is acceptable only when the depth to top is less than or equal to it. However, and in all the studied models, the larger side of the body is not at all affected by the depth variation.

7. Depth estimation

We have shown that the distance between two extremities on the VLF-EM map or on the X-derivative one (ΔY), and the zero-crossing distance in the Y-derivative map, are the same as the known peak-to-peak distance (ΔX) normally used in VLF-EM interpretation to estimate the depth to top of a body (Paterson and Ronka, 1971; Coney, 1977; Baker and Myers, 1979). But the relationships between ΔX and the depth developed by these authors to estimate the depth to top is based on 2D VLF-EM models and only gives an acceptable result if the ratio a/b verifies the condition $a/b \geq 10$ for thin tabular conductors (where a and b are the calculated dimensions of the body in the X and Y directions), and that the strike of the causative body is parallel to the propagation direction. However, the results obtained here with the 3D modelling are used to plot a similar relationship that could be useful in estimating the depth to top of any target regardless to its position, and with any possible a/b ratio. Three family curves were obtained (fig. 9 and table II):

- The first family for $a \gg b$.
- The second family for $a = b$.
- The third family for $a \ll b$.

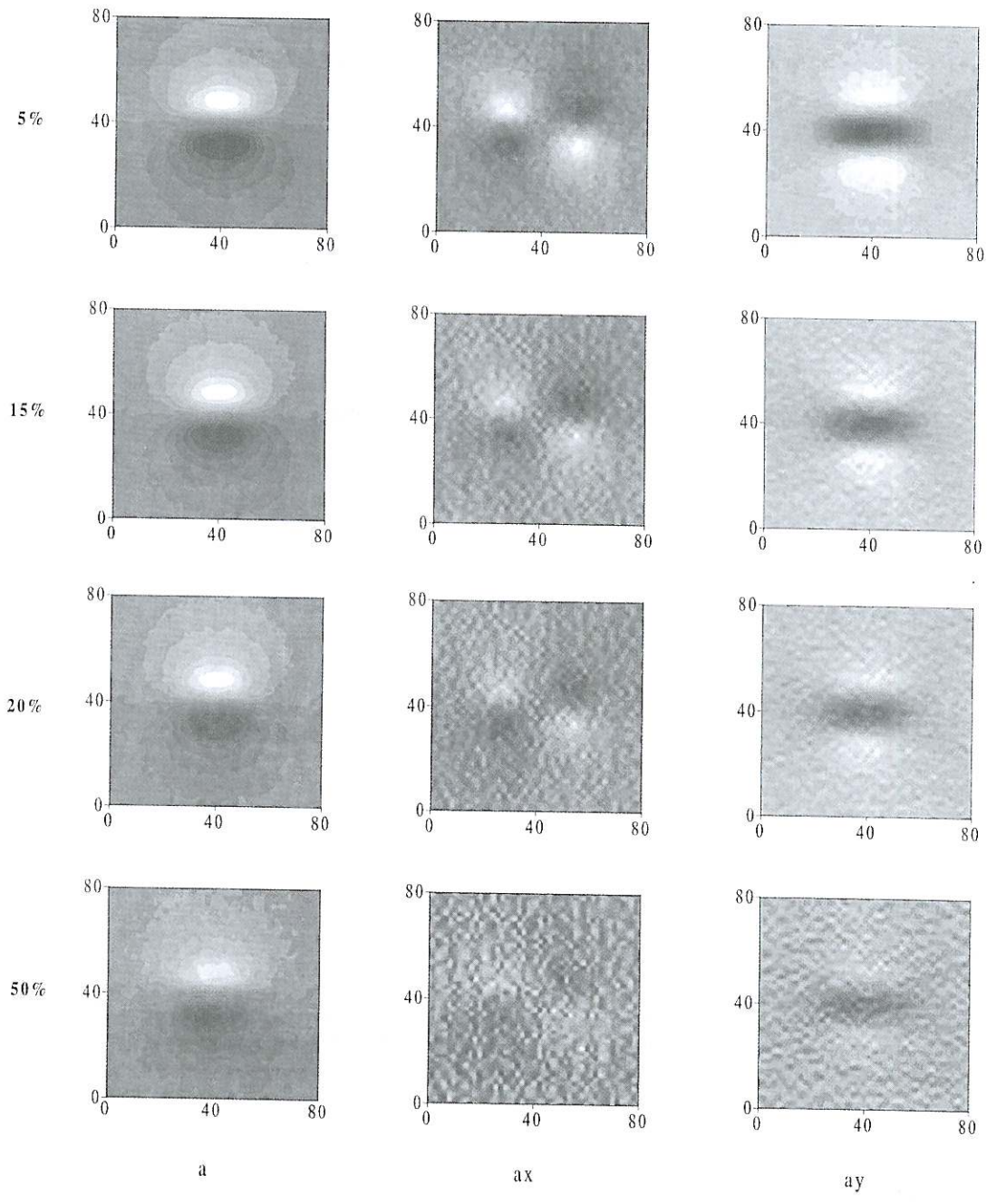

Fig. 7. a = Real (H_x/H_y) maps with different percentages of noise/signal ratio; a_x = X-derivative maps; a_y = Y-derivative maps.

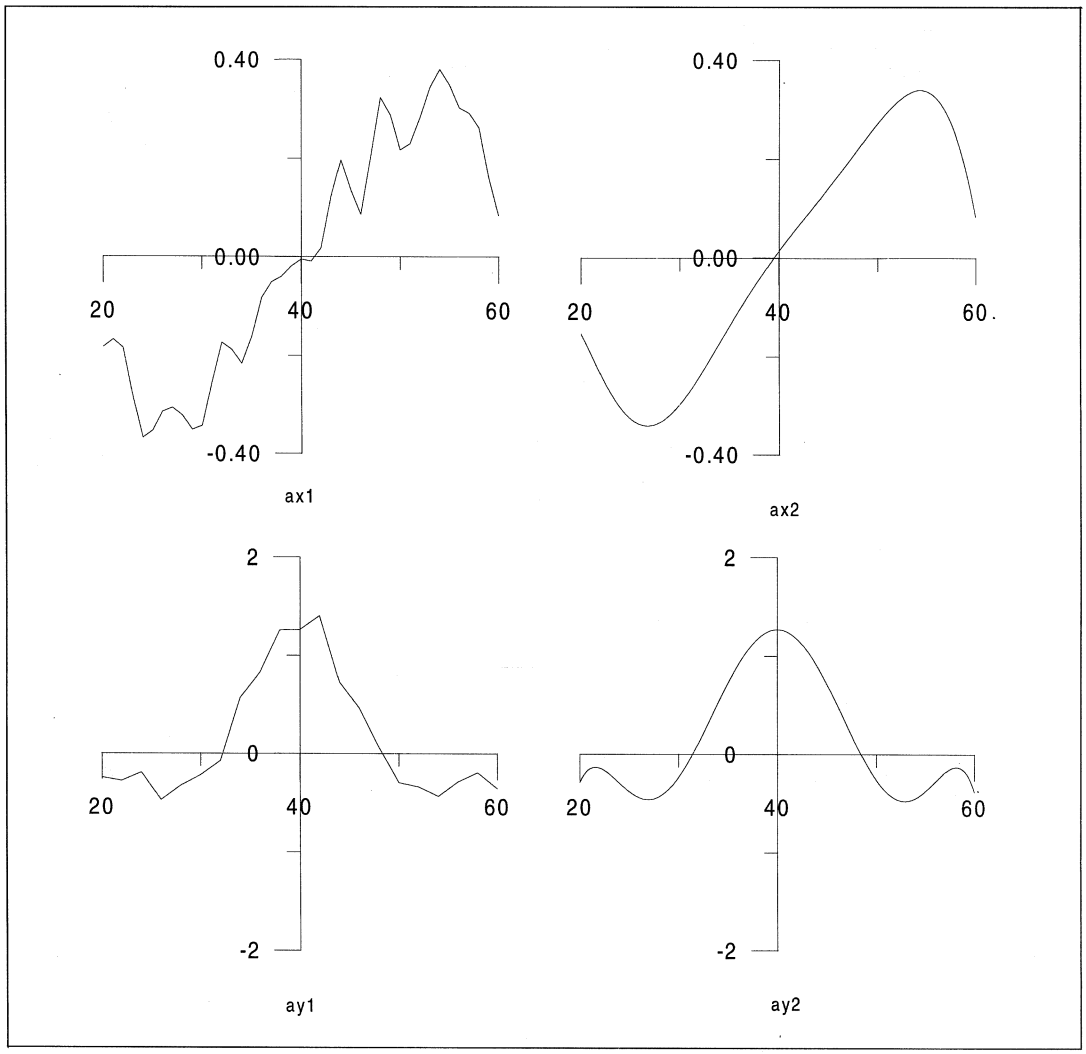

Fig. 8. Profiles along the X- and Y-derivative maps of the 15% noise/signal ratio. a_{x1} = Profiles on the X-derivative map before interpolation at $Y = 35$; a_{y1} = profile on the Y-derivative map before interpolation at $X = 40$; a_{x2} and a_{y2} the same profiles after interpolation.

From fig. 9, we observe that in the first family curves, the increase in a/b ratio does not affect the curve and an insignificant difference is noted for various ratios of a/b. This is true only if the body has a strike perpendicular to the primary field. This means that the conditions are similar to those given in the above mentioned authors' models. And for comparison, we noted that the Baker and Myers curve is partially similar to the first family curves.

But when the body strike is parallel to the primary magnetic field, we obtain the third

Table I. Variation of length estimation at variable depth for different orientations of a 3D target.

Body with	Depth to top (m)	*XL* calculated (m)	*YL* calculated (m)
	4	19	5
XL = 20	5	19	5
YL = 5	6	19	6
ZL = 6	8	19	8
	10	20	10
	4	5	20
XL = 5	5	5	20
YL = 20	6	6	21
ZL = 6	8	10	22
	10	11	24

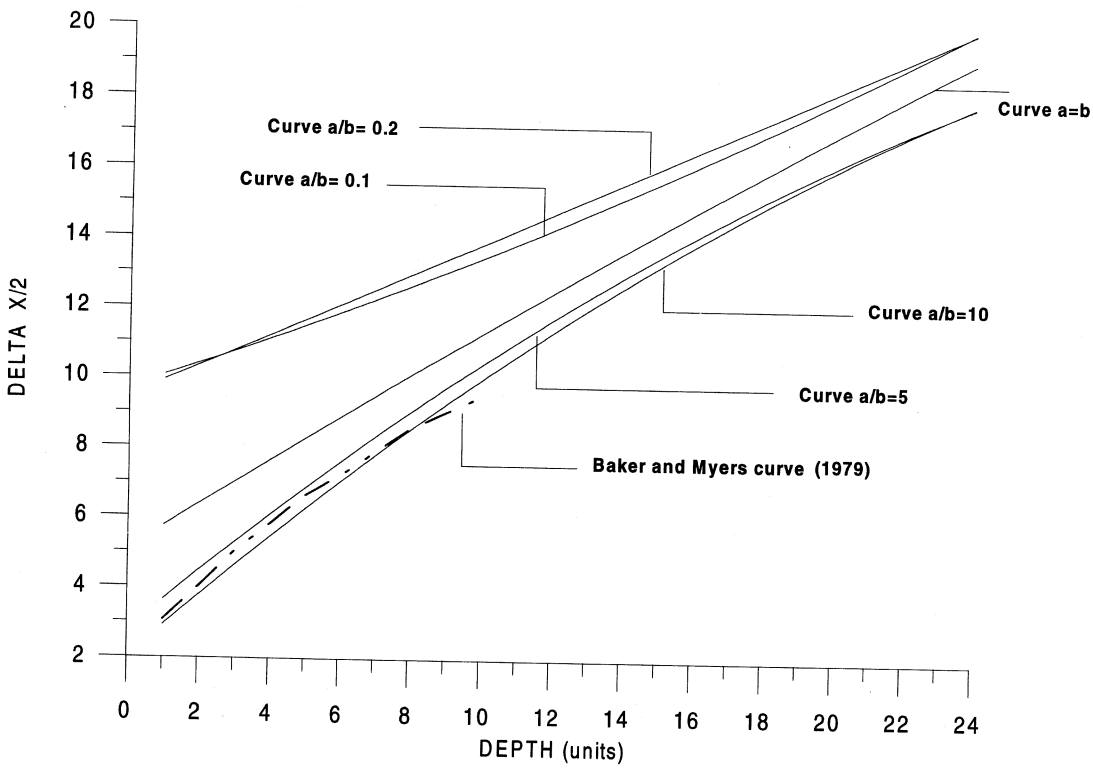

Fig. 9. Relationship between $\Delta X/2$ and depths of body for different ratio of a/b. a and b are body dimensions along X and Y-axes respectively.

Table II. The parameters used to draw fig. 9.

Depth to top	$\Delta X/2$ for different a/b					Baker and Myers
	a/b = 0.1	a/b = 0.2	a/b = 1	a/b = 5	a/b = 10	
1	10	10	6	4	2	3
2	10	10	6	4	4	4
3	11	11	7	5	5	5
4	11	11	8	6	6	5.8
5	12	12	8	7	6	6.6
6	12	12	9	8	7	7.2
8	12	13	10	9	9	8.5
10	14	14	11	10	10	9.5
12	14	14	12	12	11	
14	15	16	14	13	12	
16	16	16	15	14	14	
18	17	18	16	15	15	
20	18	18	17	16	16	
22	19	19	18	17	17	
24	20	20	19	18	18	

family curves. In this case, a significant increase in b/a will have a very small effect on the curve.

The second family curve is a straight line that can be considered an intermediate case.

If the ratio a/b is far superior to 10, then the first family curves can always be used to obtain a good estimation of the depth. And if a ratio of a/b is obtained other than the ones given in fig. 9, in this case an interpolation between two successive family curves would be necessary.

8. Conclusions

The utilisation of the first derivative in the direction of the primary magnetic and electric fields gives the exact positioning of the target as well as its real dimensions. This is only true if the depth to top of the structure does not exceed the smallest extension of the body in the XY-plane. However, an acceptable estimation of its dimensions can always be obtained. The linear filter gives also good results if the noise/signal ratio is equal to or less than 15%. Moreover, the recognition of the body dimensions is possible even when this ratio is superior to 15%.

On the one hand, the introduction of this approach opens a new opportunity in using the VLF-EM method not only in mining exploration, but also in other shallow geophysical studies, *e.g.*, civil engineering, archaeology, etc. On the other hand, the utilisation of this method is not limited to locating conductive bodies only, but the topographical effect is also negligible since in applying the proposed filter we only theoretically consider the inflection points on the VLF-EM anomaly.

The adaptation of the Fraser filter in studying 3D bodies, and the observed similarity of results with those obtained by the derivatives also indicate a quantitative application of the Fraser filter.

REFERENCES

BAKER, H.A. and J.O. MYERS (1979): VLF-EM model studies and some simple quantitative applications to field results, *Geoexploration* **17**, 55-63.

CHOUTEAU, M., P. ZHANG and D. CHAPELIER (1996): Computation of apparent resistivity profiles from VLF-EM data using linear filtering, *Geophys. Prospect.*, **44**, 215-232.

CONEY, D.P. (1977): Model studies of the VLF-EM method of geophysical prospecting, *Geoexploration*, **15**, 19-35.

FRASER, D.C. (1969): Contouring of VLF-EM data, *Geophysics*, **34**, 958-967.

GUERIN, R., A. TABBAGH and P. ANDRIEUX (1994): Field and/or resistivity mapping in MT-VLF and implications for data processing, *Geophysics*, **59**, 1695-1712.

GUERIN, R., A. TABBAGH, Y. BENDERITTER and P. ANDRIEUX (1994): Invariants for correcting field polarisation effect in MT-VLF resistivity mapping, *J. Appl. Geophy.*, **32**, 375-383.

KAROUS, M. and S.E. HJELT (1983): Linear filtering of VLF dip-measurement, *Geophys. Prospect.* **31**,782-794.

MCNEIL, J.D. (1985): The galvanic current component in electromagnetic surveys, *Technical Note TN-17* (Geonics Limited, Mississauga, Ontario, Canada).

OGILVY, R.D. and A.C. LEE (1991): Interpretation of VLF-EM in-phase data using current density pseudosections, *Geophys. Prospect.*, **39**, 567-580.

PATERSON, N.R. and V. RONKA (1971): Five years of surveying with the very low frequency electromagnetic method, *Geoexploration*, **9**, 7-26.

TABBAGH, A. (1985): The response of a three-dimensional magnetic and conductive body in shallow depth electromagnetic prospection, *Geophys. J. R. Astron. Soc.*, **81** (1), 215-230.

TABBAGH, A., Y. BENDRITTER, P. ANDRIEUX, J.P. DECRIAUD and R. GUERIN (1991): VLF resistivity mapping and verticalization of the electric field, *Geophys. Prospect.*, **39**, 1083-1097.

(received November 21, 1997;
accepted June 26, 1998)